Springer Tracts in Modern Physics
181

J. Bibette
F. Leal-Calderon
V. Schmitt
P. Poulin

Emulsion Science

Basic Principles
An Overview

Springer Tracts in Modern Physics
Volume 181

Now also Available Online

Starting with Volume 165, Springer Tracts in Modern Physics is part of the Springer LINK service. For all customers with standing orders for Springer Tracts in Modern Physics we offer the full text in electronic form via LINK free of charge. Please contact your librarian who can receive a password for free access to the full articles by registration at:

http://link.springer.de/series/stmp/reg_form.htm

If you do not have a standing order you can nevertheless browse through the table of contents of the volumes and the abstracts of each article at:

http://link.springer.de/series/stmp/

There you will also find more information about the series.

Springer
Berlin
Heidelberg
New York
Hong Kong
London
Milan
Paris
Tokyo

Physics and Astronomy ONLINE LIBRARY
http://www.springer.de/phys/

Springer Tracts in Modern Physics

Springer Tracts in Modern Physics provides comprehensive and critical reviews of topics of current interest in physics. The following fields are emphasized: elementary particle physics, solid-state physics, complex systems, and fundamental astrophysics.
Suitable reviews of other fields can also be accepted. The editors encourage prospective authors to correspond with them in advance of submitting an article. For reviews of topics belonging to the above mentioned fields, they should address the responsible editor, otherwise the managing editor.
See also http://www.springer.de/phys/books/stmp.html

J. Bibette
F. Leal-Calderon
V. Schmitt
P. Poulin

Emulsion Science

Basic Principles.
An Overview

With 50 Figures

Springer

Professor Jerome Bibette
ESPCI
Laboratoire Colloides
et Nanostructures
10, rue Vauquelin
75231 Paris cedex 05, France
E-mail: jerome.bibette@espci.fr

Professor Fernando Leal-Calderon
University of Bordeaux 1
Institut des Sciences et Techniques
des Aliments de Bordeaux
Avenue des Facultés
33405 Talence, France
E-mail:lealcalderon@free.fr

Dr. Veronique Schmitt
University of Bordeaux 1
Centre de Recherche Paul Pascal
Avenue Albert Schweitzer
33600 Pessac, France
E-mail: schmitt@crpp.u-bordeaux.fr

Dr. Philippe Poulin
University of Bordeaux 1
Centre de Recherche Paul Pascal
Avenue Albert Schweitzer
33600 Pessac, France
E-mail: poulin@crpp.u-bordeaux.fr

Library of Congress Cataloging-in-Publication Data.

Emulsion science: basic principles. an overview/Jerome Bibette... [et al.].
p.cm. – (Springer tracts in modern physics, ISSN 0081-3869; v. 181)
Includes bibliographical references and index.
ISBN 3-540-43682-0 (acid-free paper)
1. Emulsions. I. Bibette, Jerome, 1960– . II. Springer tracts in modern physics; 181.
QC1.S797 vol. 181 [TP156.E6] 539 s–dc21 [541.3'4514] 2002090667

Physics and Astronomy Classification Scheme (PACS):
82.70.Kj, 82.70.-y, 68.05.-n, 68.15.+e

ISSN print edition: 0081-3869
ISSN electronic edition: 1615-0430
ISBN 3-540-43682-0 Springer-Verlag Berlin Heidelberg New York

Springer-Verlag Berlin Heidelberg New York
a member of BertelsmannSpringer Science+Business Media GmbH

http://www.springer.de

Printed in Germany

Typesetting: Data conversion by Da-TEX, Gerd Blumenstein, Leipzig
Cover design: *design & production* GmbH, Heidelberg

Printed on acid-free paper SPIN: 10791158 56/3141/tr 5 4 3 2 1 0

Preface

Emulsions occur either as end products or during the processing of products in a huge range of areas including the food, agrochemical, pharmaceuticals, paints and oil industries. As end products, emulsions allow to avoid organic solvent in processing hydrophobic coatings. Emulsion technology is a suitable approach to vehicle viscous phases. It is also a remarkable mean of targeting actives or capturing specific species. The range of applications of emulsions progresses and their manufacturing becomes more and more sophisticated.

Besides this broad domain of technological interest, emulsions are raising a variety of fundamental questions at the frontier between physic and chemistry. Indeed, as a class of soft colloidal materials, emulsions science is linked to various aspects of these disciplines: phase transitions, surface forces and wetting, metastability and hydrodynamic instabilities, mechanical properties and flow.

The aim of this book is to review the main important concepts governing emulsion science. In Chapter 2, repulsive interactions between liquid films are discussed as well as adhesive interaction related to wetting. In Chapter 3, consequences of weak and strong attractions are presented, related to the well accepted liquid–solid transition analogy. In Chapter 4, the basics of both bulk compressibility and shear elasticity are presented, the role of disorder being the most important aspect of the elastic behavior of these soft systems. In Chapter 5 the central question of the emulsion lifetime related to metastability is discussed. The various scenarios of destruction are presented in relation with their various microscopic mechanisms. In Chapter 6, the fabrication of monodisperse emulsions from Raleigh instability in controlled shear is explained. Finally, Chapter 7 give the basic principles of double emulsions related to their potential use in pharmaceutical applications.

We believe this book is reporting most of the progress of these last 15 years. It should be helpful for Phd students aiming to get the basics of emulsion science for further research in this field as well as for engineers working on new applications of these materials.

Paris, July 2002 *Jérôme Bibette*

Contents

3 Phase Transitions

3.1 Weak Attractive Interactions and Equilibrium Phase Transitions

Attractive interactions between droplets may induce reversible phase transitions or flocculation and depending upon the densities of the solvent and the droplets, sedimentation or creaming occurs. Flocculation is a process in which emulsion droplets aggregate, without rupture of the stabilizing film between them. Flocculation occurs when the total pair interaction between the droplets becomes appreciably attractive at some separation. If the depth of the attractive well is of the order of kT, then the droplets form aggregates which coexist with single Brownian droplets. The thermal energy allows an equilibrium state to be reached, with continual exchange between aggregated and free droplets. On the macroscopic scale, after a few hours of settling, the emulsion undergoes a phase separation into a concentrated cream or sediment and a dilute phase. When the depth of the attractive well is large compared with kT (i.e. more than $10kT$), the droplets are strongly bound to the aggregates and cannot be redispersed by thermal motion. After a short period of time, all the droplets are entrapped within large, tenuous clusters that fill the whole space. The contraction of this gel-like network may take a very long time, especially in concentrated emulsions. In this section, we shall describe reversible flocculation phenomena, while irreversible flocculation phenomena and their associated gel structures will be presented in Sect. 3.2.

3.1.1 Experimental Observations

Oil-in-Water Emulsions. Reversible flocculation may be produced simply by adding excess surfactant to the continuous phase of an emulsion. As already mentioned in the previous chapter, micelles may induce an attractive depletion interaction between the oil droplets. For spheres of equal radius R at a center-to-center separation r, the depletion energy may be written as [1]

$$u_{\mathrm{d}} = \int_{\infty}^{r} F(r')\,\mathrm{d}r' = -\frac{4\pi}{3}(R+\Delta)^3 P_{\mathrm{osm}} \left[1 - \frac{3r}{4(R+\Delta)} + \frac{r^3}{16(R+\Delta)^3}\right], \tag{3.1}$$

Bibette, Leal-Calderon, Schmitt, Poulin: Emulsion Science, STMP 181, 47–65 (2002)

where Δ is a characteristic exclusion length, which may be assumed to be the micellar radius, and P_{osm} is the micellar osmotic pressure. This potential decreases monotically from zero at $r = 2(R + \Delta)$ to a minimum at contact ($r = 2R$):

$$u_{\mathrm{c}} = -\frac{4\pi\Delta^3}{3}\left(1 + \frac{3R}{2\Delta}\right) P_{\mathrm{osm}}\,. \tag{3.2}$$

The first observations of depletion flocculation by surfactant micelles were reported by Aronson [2]. Bibette and coworkers [3] have studied the behavior of silicone-in-water emulsions stabilized by SDS (sodium dodecyl sulfate). These authors exploited the attractive depletion interaction to size-fractionate a crude polydisperse emulsion [4]. Since the surfactant volume fraction necessary to induce flocculation is always lower than 5%, the micelle osmotic pressure can be taken to be the ideal-gas value:

$$P_{\mathrm{osm}} \approx n_{\mathrm{m}} kT = \frac{\phi_{\mathrm{m}}}{4/3\pi\Delta^3} kT\,, \tag{3.3}$$

where n_{m} and ϕ_{m} are the micelle concentration and volume fraction, respectively. Moreover, since the silicone oil droplets have sizes ranging from 0.1 µm to a few microns, the ratio a/Δ is very large and (3.2) can be approximated by

$$u_{\mathrm{c}} \approx -\frac{3}{2} kT \phi_{\mathrm{m}} \frac{R}{\Delta}\,. \tag{3.4}$$

This equation predicts a simple linear dependence of the contact potential on the micelle volume fraction and on the ratio R/Δ. For example, for $\phi_{\mathrm{m}} = 1\%$, this equation predicts that the pair contact energy between oil droplets having a radius of 0.5 µm is equal to $4kT$, an attraction which is in principle sufficient to produce flocculation. By adjusting the concentration of surfactant above its CMC value, the volume fraction of micelles can be easily controlled. To produce monodisperse emulsions, a crude polydisperse emulsion can be diluted to a droplet volume fraction of $\varphi_{\mathrm{d}} \approx 0.1$. According to (3.4), for any given micelle volume fraction ϕ_{m}, the magnitude of the depletion attraction will be greater than kT for oil droplets larger than some radius and will cause these larger droplets to flocculate. The density mismatch between the oil and the water will cause these flocs to cream after approximately 12 h of settling. The creamed droplets can be removed from the initial emulsion and redispersed at $\varphi_{\mathrm{d}} \approx 0.1$ in a separate suspension. By this means, the droplet distribution has been divided into two parts; droplets larger than some size are preferentially in one part, while smaller droplets are in the other part. For the second fractionation step, the surfactant concentration of the emulsion containing the large droplets is reduced in order to flocculate only the largest droplets. For the daughter emulsion containing the smaller droplets, the surfactant concentration is raised to flocculate still

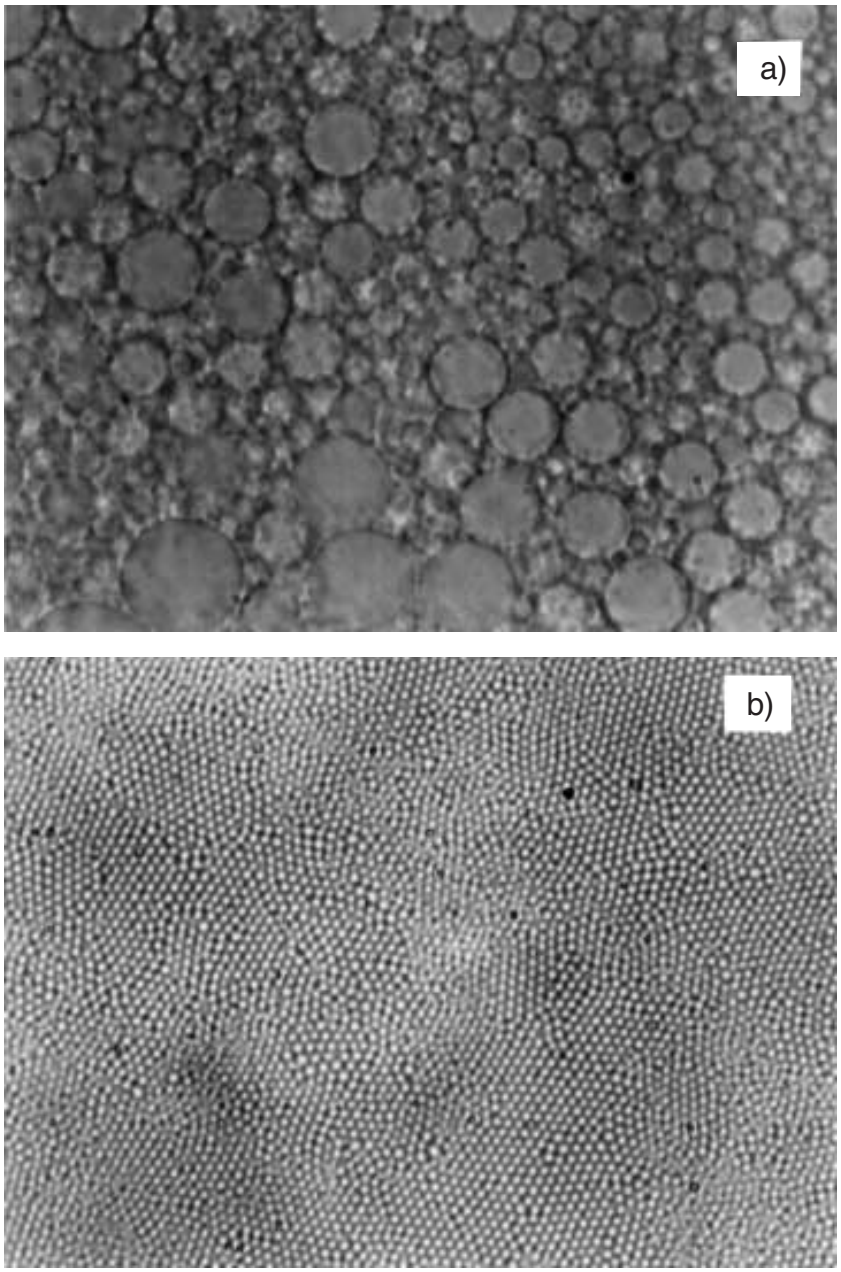

Fig. 3.1. Microscope image of a polydisperse emulsion (**a**) and of the emulsion obtained after 6 fractionation steps (**b**). The droplet volume fraction in both pictures is around 60%

smaller droplets. By repeating this separation procedure five or six times, several monodisperse emulsions having different droplet radii can be fractionated from a single polydisperse emulsion.

The uniformity of the droplet size distribution can be seen by comparing an initial polydisperse emulsion, shown in the optical microscope image in Fig. 3.1a, with a monodisperse emulsion at the same volume fraction ($\approx 60\%$)

obtained after six purification steps, shown in Fig. 3.1b. The polydisperse emulsion is highly disordered and possesses a wide range of droplet sizes. By contrast, the droplet size of the purified emulsion is very uniform, allowing the development of ordered packing. This fractionation method can produce monodisperse emulsions with droplet radii that range from $R = 0.1\,\mu\text{m}$ to $R = 1\,\mu\text{m}$. The degree of polydispersity (defined as the ratio of the size distribution's width to its average) may be as low as 10% after six purification steps. Owing to the entropic origin of the depletion attraction, this method is applicable to any kind of emulsion stabilized by any kind of surfactant provided the emulsion is stable against coalescence and Ostwald ripening.

Once produced, monodisperse emulsions can be used to study the physics of the phase separation that occurs in the presence of excess surfactant [5]. As previously described, adding surfactant leads to the formation of aggregates coexisting with free droplets. Likewise, the two coexisting phases, the dense one containing aggregates and the dilute one containing free droplets, continuously exchange particles, as can be observed under a microscope (Fig. 3.2). This strongly suggests the existence of a fluid–solid thermodynamic equilibrium like that defined in the field of conventional molecular fluids. Macroscopic samples of the dense phase may be obtained after decantation. Iridescence is observed when a 1–5 mm thick film of this dense phase is deposited between two glass slides. This property gives fairly good evidence that the dense phase is solid-like, with long-range ordering of the oil droplets. This is confirmed by the microscope picture of Fig. 3.1b, in which one can easily distinguish oil droplets forming randomly oriented crystallites, and by

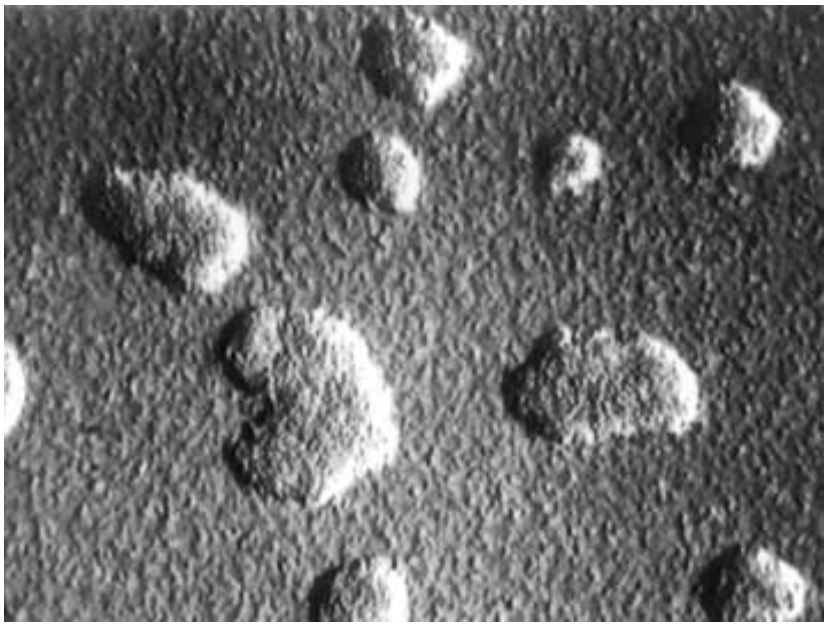

Fig. 3.2. Microscope image showing the effect of adding excess surfactant to the continuous phase of the emulsion: flocs separate from a coexisting fluid phase

light diffraction experiments, the results of which are consistent with a face-centered crystalline structure [5]. Since a thermodynamic equilibrium is expected, one can draw a phase diagram for various droplet sizes as a function of surfactant concentration and oil droplet volume fraction [5] (Fig. 3.3). The experimental points separate the one-phase region, where only free droplets are observed, from the two-phase region, where aggregated and free droplets coexist. The so-called creaming effect is systematically observed at the macroscopic level when the surfactant concentration threshold is reached. Qualitatively, the depletion mechanism is consistent with the droplet size dependence of the experimental phase diagrams. Indeed, the aggregation of a colloid at low droplet volume fraction can be considered as a gas–solid phase transition and may be described simply by equating both the chemical potentials and the pressures of an ideal gas and of a purely incompressible dense phase involving only nearest neighbors: $\ln \varphi_{\mathrm{d}} = (z/2kT)(u_{\mathrm{c}} + \Delta\mu^0)$, where z is the coordination number of a droplet within the dense phase, φ_{d} is the droplet volume fraction, and $\Delta\mu^0$ is the reference chemical-potential difference between the fluid and dense phases. Therefore, it can be assumed that at constant oil volume fraction, the boundary corresponds to a constant contact pair interaction between droplets within the aggregates. Therefore, from (3.4), higher ϕ_{m} values are required for smaller droplets to obtain phase separation, as observed experimentally. The colloidal structure of dilute phases has been investigated by means of static light-scattering experiments [5]. The dilute

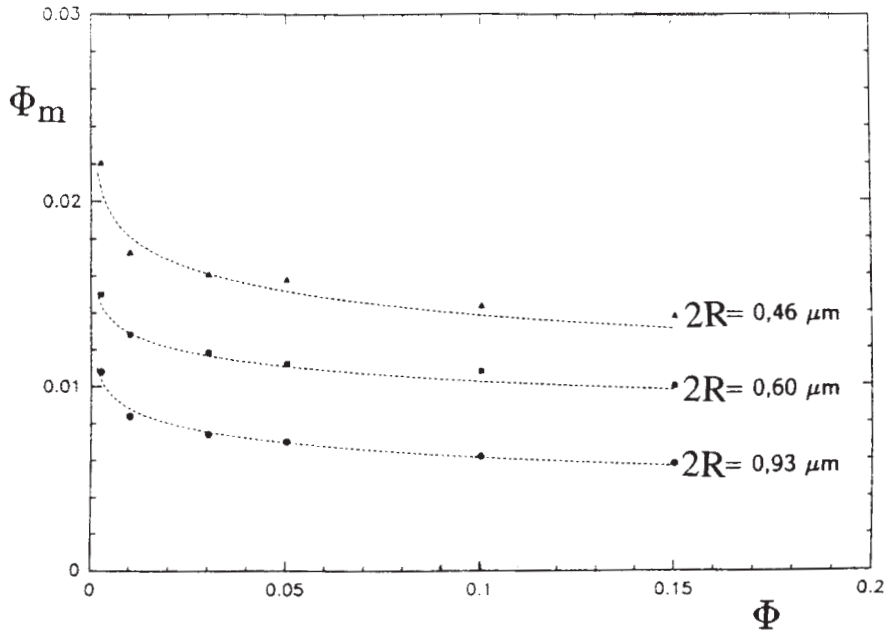

Fig. 3.3. Experimental phase diagrams in the micelle volume fraction ϕ_{m}/oil volume fraction ϕ plane. The *lines* are guides to the eyes that delimit the one-phase region (fluid) from the two-phase region (fluid + solid)

phase exhibits a correlation peak indicating hard-sphere-like interactions between emulsion droplets at low surfactant concentration, replaced by intense small-angle scattering indicative of attractive interactions at higher surfactant concentration. The attractive interactions deduced from the scattered intensity profiles confirm the depletion mechanism.

Meller and Stavans have investigated the effect of nonadsorbing hydrophilic polymers (poly(ethylene oxide)) on the stability of monodisperse oil-in-water emulsions [6]. Above some threshold polymer concentration, the polymer coils induce a fluid–solid equilibrium owing to depletion effects. In the dilute regime, macromolecules may be regarded as hard spheres of radius R_g, which are excluded when the droplet surface separation becomes lower than $\Delta = R_g$. Steiner et al. have investigated the phase behavior of mixtures of emulsion droplets having two sizes, covering a large range of relative compositions and size ratios [7]. Their results confirm the general phenomenology of phase separation induced by osmotic depletion forces, induced in turn by the smaller droplets. From Steiner et al.'s study, it may be concluded that polydispersity in itself may induce creaming.

Reversible flocculation may also be observed in emulsions stabilized by nonionic surfactants when the temperature is increased. It is well known that many nonionic surfactants dissolved in water undergo a phase separation: above a critical temperature, an initially homogeneous surfactant solution separates into two micellar phases of different composition. This demixing is generally termed the "cloud point transition". Similarly, oil droplets covered by molecules of the surfactant become attractive around the same temperature and undergo a reversible fluid–solid phase separation [8].

Water-in-Oil Emulsions. Inverted emulsions are generally made of water droplets covered by a layer of short, aliphatic chains adsorbed at the oil–water interface. Since the droplets are not charged and ions do not form easily in low-dielectric-constant organic solvents, electrostatic interaction can be neglected. Thus the interaction between the droplets depends essentially on the London–van der Waals forces between the droplet cores and on the quality of the solvent with regard to the stabilizing chains. A rough approximation of the van der Waals potential between spherical particles in contact is given by $u_{\mathrm{vdW}} = -(AR/24\delta)$ [9], where A is the Hamaker constant and δ is the thickness of the surfactant stabilizing layer. To impart stability against van der Waals attraction, this interaction potential must be of the order of or lower than the thermal energy kT. For this to be the case, the stabilizing thickness δ must satisfy the condition

$$\frac{\delta}{R} \geq \frac{A}{24kT} \,. \tag{3.5}$$

The interaction that arises from the overlapping of the surfactant chains is due to a complex interplay between enthalpic and entropic effects involving surfactant chain segments (monomer units) and solvent molecules. The en-

thalpic part of the interaction is determined by the balance between segment–segment and solvent–segment interactions. If the latter are highly favorable, the chains are solvated by solvent molecules and a slight interpenetration of two stabilizing layers leads to a strong repulsion, which can be modeled as a "hard sphere" interaction. This repulsion is very strong and short-ranged because the chains are short and uniform in length, and cover the surface densely. If the segment–solvent interaction is unfavorable, then in addition to the usual steric repulsion, an attractive interaction may appear between the stabilizing chains.

Leal-Calderon et al. [10] have studied the flocculation of water-in-oil emulsions stabilized by Span 80 (sorbitan monooleate, which possesses an unsaturated average C_{18} hydrophobic tail), a low HLB surfactant. Above the critical micellar concentration, inverted micelles are present within the continuous oil phase, thus allowing micellar depletion forces to induce reversible flocculation and further fractionation of crude polydisperse emulsions. In several decantation steps, a set of different monodisperse emulsions can be obtained using the same procedure as described for direct emulsions. The monodisperse samples can then be used to characterize the role of the continuous oil phase in inducing aggregation. It appears that the droplets are dispersed in some oils, referred to as "good solvents", such as dodecane, and remain aggregated in many other oils, referred to as "bad solvents", such as like vegetable or silicone oils. Hence, it is interesting to identify and characterize the aggregation threshold as a function of the composition of a continuous phase made of a mixture of a good solvent (dodecane) and a bad solvent (a fatty ester, isopropyl myristate). Figure 3.4b shows the phase diagram obtained when the contents of both the surfactant and the second solvent (isopropyl myristate) are varied at constant water droplet volume fraction (5%). The system changes continuously from a Brownian emulsion to a gel with the addition of isopropyl myristate or excess surfactant. For intermediate solvent compositions, coexisting states (fluid–solid equilibrium) are observed. It is also noteworthy that this threshold depends upon the droplet size. Indeed, aggregation is found at lower surfactant or isopropyl myristate contents as the droplet diameter is increased (Fig. 3.4a). In other words, a smaller amount of surfactant or of the bad solvent is required for larger droplets to phase-separate. Figure 3.5 shows a microscope picture of an emulsion in which the solvent composition is much above the aggregation threshold. As shown by this picture, the shape of the clusters in this emulsion is very tenuous. These clusters are very reminiscent of those observed in direct emulsions undergoing gelation upon addition of an electrolyte. Such an observation suggests that the attractive interaction between water droplets induced by the addition of the second solvent may become much larger than kT.

As in the case of direct emulsions, the presence of excess surfactant induces a depletion interaction followed by phase separation. Such a mechanism was invoked by Binks et al. [11] to explain the flocculation of inverted emulsion

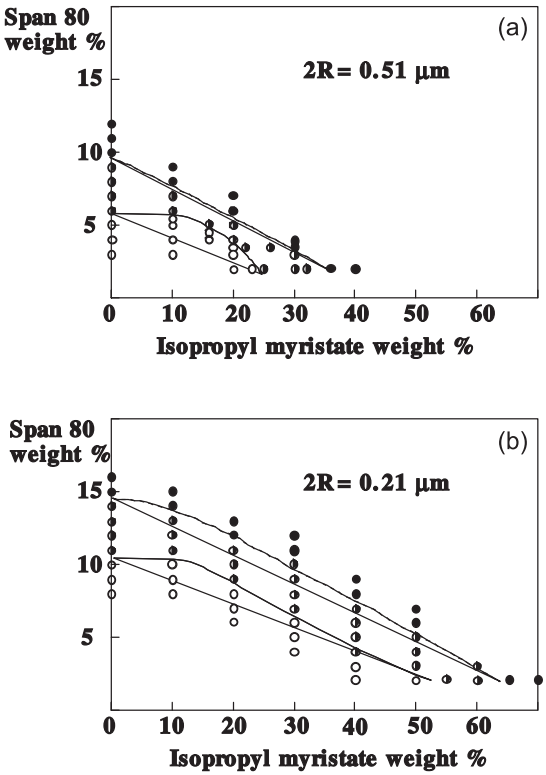

Fig. 3.4. Phase diagrams obtained for two monodisperse emulsions. ∘ Totally dispersed; ∅ flocculated (fluid–solid equilibrium); • totally floculated (gel)

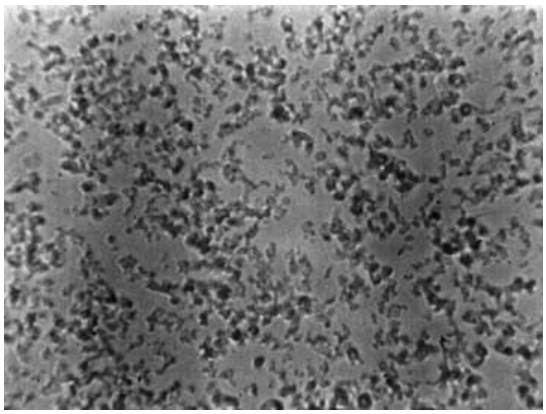

Fig. 3.5. Microscope image of a totally flocculated emulsion (water droplets 0.4 µm in size in $C_{26}H_{54}$, $T = 65\,^{\circ}C$)

droplets in the presence of microemulsion-swollen micelles. The microscopic origin of the interaction driven by the presence of the "bad solvent" is more speculative. From empirical considerations, it can be deduced that surfactant chains mix more easily with mineral oil than with vegetable, silicone, and some functionalized oils. The size dependence of such a mechanism, reflected by the shifts in the phase transition thresholds, is certainly due to the

increasing contact surface between larger droplets. As already mentioned, the interactions between the stabilizing chains are quite complex and rather sensitive to many different microscopic parameters, such as segment–segment and chain–solvent molecular interactions, surfactant coverage, the thickness of the adsorbed layer, and the solvent chain length.

Leal-Calderon et al. [12] have proposed some basic ideas to describe the colloidal interactions induced by a solvent or a mixture of solvent and solute, when the length n of the solvent molecules is varied from a molecular scale to a colloidal scale. These authors have investigated the behavior of water- and glycerol-in-oil emulsions in the presence of linear flexible chains of various masses. Figure 3.6 shows the phase behavior of both water and glycerol droplets when dispersed in a linear aliphatic solvent of formula C_nH_{2n+2}, where $n = 5$ to 30. Since for n larger than 16 solvent crystallization occurs at room temperature, a second series of experiments was performed at 65 °C. The absolute value of the refractive-index mismatch Δn_r between the oil and water or glycerol is plotted as a function of n. The state of aggregation is reported for each sample (filled symbols, aggregated; empty symbols, dispersed). For water droplets, increasing n leads to an increase in $|\Delta n_r|$ and an aggregation threshold appears at large n. Below this threshold, occurring at $n = 24$, the droplets are perfectly Brownian, while above the threshold, the emulsions turn into a completely aggregated system. In contrast, for glycerol droplets, increasing n reduces $|\Delta n_r|$ and, instead, two distinct thresholds at $n = 7$ and $n = 26$ are observed. The droplets are first aggregated ($|\Delta n_r|$ large), become dispersed as $|\Delta n_r|$ reduces, and are finally aggregated again as $|\Delta n_r|$ reduces further. Note that this second aggregation threshold occurs in the limit of large n.

From these results, it can be concluded that two distinct, independent mechanisms affect the colloidal aggregation and therefore the contact pair interaction. One mechanism is controlled by the refractive-index mismatch,

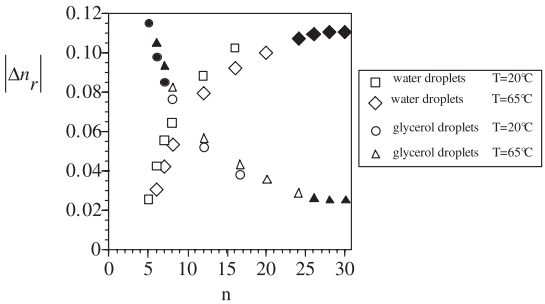

Fig. 3.6. State of aggregation of water and glycerol droplets in different oils (C_nH_{2n+2}) as a function of n and of the absolute value of the refractive-index mismatch Δn_r between the dispersed and the continuous phase. The surfactant concentration (Span 80) is equal to 1% by weight. The droplet volume fraction is set at 5%. The water and glycerol droplets have a diameter close to 0.4 µm. *Filled symbols*, aggregated droplets; *empty symbols*: dispersed droplets

which reflects the magnitude of the van der Waals forces. The hydrocarbon–water Hamaker constant lies in the range $3\text{–}7\times10^{-21}$ J [9] when n varies from 5 to 30. Assuming a layer thickness δ of about 2 nm, the above relation gives a potential energy between 2 and $6kT$, a range in which phase separation is expected to occur, as found experimentally for water droplets. However, for glycerol droplets, the Hamaker constant decreases continuously as n increases and the flocculation observed for $n > 26$ makes us fairly certain that the attraction in the presence of long alkanes is not produced only by van der Waals forces. The interaction that arises from the overlapping of the surfactant chains covering the droplets is controlled by the chain length of the solvent, which certainly suggests an entropically driven mechanism. Indeed, enthalpic contributions to the non-van der Waals forces should change only weakly as n varies because the chemical nature of the solvent remains the same (alkanes), and the surfactant chain is also kept the same.

To test this idea, the coupling between the length parameter n and the volume fraction ϕ of flexible chains when mixed with dodecane was investigated. Because the variable ϕ allows one to continuously vary the magnitude of the attraction, it is possible to induce a transition from the dispersed to the totally aggregated state with a coexisting state in between (fluid–solid equilibrium). Figure 3.7 shows the aggregation threshold ϕ^* of glycerol droplets ($\varphi_d = 5\%$) in the ϕ/n plane from $n = 25$ to $n = 40$. ϕ^* is defined as the volume fraction of the linear alkane C_nH_{2n+2} required to reach the coexisting state. Observations were performed at 65 °C in order to avoid any crystal-

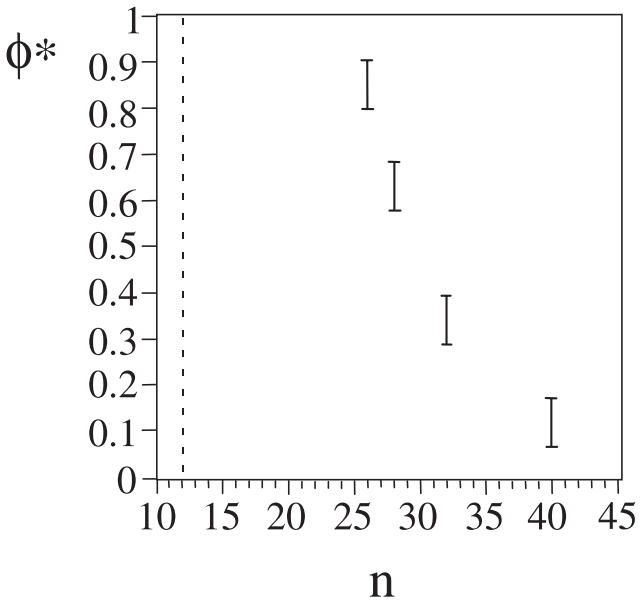

Fig. 3.7. Volume fraction of linear alkane $C_nH_{2_n+2}$ at the onset of flocculation as a function of chain length. The continuous phase is a mixture of linear alkane, dodecane, and Span 80 (1% by weight). The glycerol droplets (5% by volume) have a diameter of 0.38 µm. $T = 65\,°C$

lization of the dodecane/C_nH_{2n+2} mixture. As expected, there is a strong coupling between ϕ and n: the longer the chain is, the fewer are required for reaching the coexisting state. Note that $\phi^*(n)$ increases dramatically when n approaches the number of unit segments that compose the adsorbed surfactant tail ($n = 18$).

In order to explore the form of the function $\phi^*(n)$ on a larger scale, the authors studied the behavior of water droplets dispersed in a mixture of polydimethylsiloxane (PDMS) chains and dodecane (with 1 wt % of Span 80). PDMS chains conform to the general formula $(CH_3)_3Si–[O–Si(CH_3)_2]_n–CH_3$. In Fig. 3.8 the concentration threshold ϕ^* of PDMS oil necessary to reach the coexisting state is plotted, as a function of the average number n of monomers per chain (at 20 °C and fixed water volume fraction $\varphi_d = 1\%$). The boundary is clearly governed by two distinct regimes: a sharp drop that occurs for low n as for alkanes, and a smoother decrease at large n. As in the case of normal alkanes, the aggregation is totally reversible, since it disappears on simple dilution with pure dodecane.

Colloidal aggregation at low droplet volume fraction can be considered as a gas–solid phase transition, and it may be assumed that the ϕ/n boundary at which colloidal aggregation occurs corresponds to a constant contact energy u of the order of kT between droplets within the dense phase (at constant φ_d of 1%). In the limit of large n ($n > 500$), a hard-core depletion mechanism may govern the evolution of the ϕ/n boundary in Fig. 3.8. The van der Waals force should remain constant, owing to the very small amount of poly-

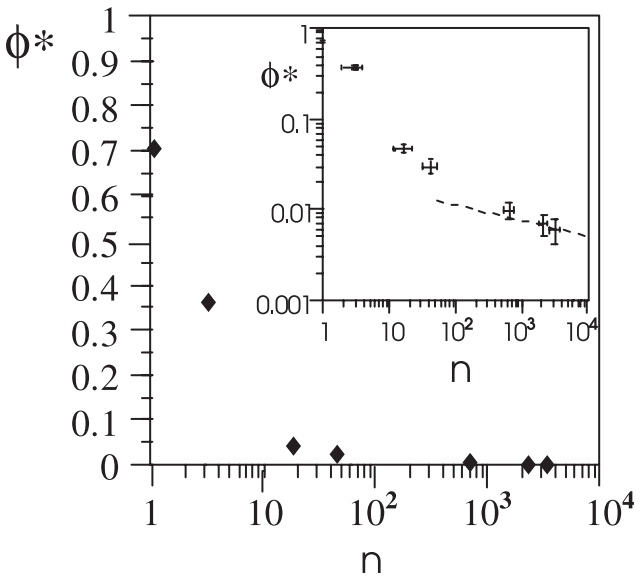

Fig. 3.8. PDMS volume fraction versus average number of unit segments at the onset of flocculation. The *dashed line* corresponds to the scaling $n^{-0.1}$ ($T = 20\,°C$; water droplet diameter = 0.28 µm; droplet volume fraction = 1%; 1% by weight of Span 80)

mer ($\phi^* < 1\%$) at which aggregation occurs. Therefore, since polymer chains are required to induce colloidal aggregation, van der Waals interactions are obviously not sufficient. However, they certainly do contribute as a constant background. The simplest description of the depletion force consists in assuming that for a droplet surface separation lower than the radius of gyration R_g, the polymer coils are totally excluded. Such mechanism leads to a contact energy u_c given by $2\pi P_{osm} R R_g^2$, where P_{osm} is the osmotic pressure of the polymer solution. This relation assumes that $R/R_g \gg 1$. Since the PDMS concentration remains very low (below the semidilute critical concentration), the perfect-gas approximation may be assumed for P_{osm}. For larger n values ($n \approx 3400$), $P_{osm} \approx 60\,\text{Pa}$ at the aggregation threshold. Using viscosimetric measurements, a hydrodynamic radius (assumed to be equal to R_g) of 147 Å has been measured at 20 °C. At such a temperature, the solvent behaves roughly as a theta solvent (the hydrodynamic radius is found to scale as n^α, where $\alpha = 0.53 \pm 0.05$ [13]). Therefore, we obtain $u_c \approx 2.7kT$, which agrees perfectly with the initial assumption: the hard-core depletion mechanism might be responsible for the evolution of the ϕ/n boundary, at least for such a large value of n. In a theta solvent, R_g scales as $n^{0.5}$ and P_{osm} as ϕ/n, and therefore the aggregation boundary in that limit should become essentially independent of n. In a good solvent, R_g scales as $n^{0.6}$, and therefore ϕ^* scales as $n^{-0.2}$. So, if the depletion interaction governs the experimental ϕ/n dependence, we expect that ϕ^* should exhibit a very weak dependence on n, which is clearly the case in the limit of large n. In the inset of Fig. 3.8 the data are plotted on a log–log plot and confirm that the slope is comparable to the expected value (between 0 and −0.2; as a guide, we have drawn a line of slope −0.1).

In the limit of small n ($n < 100$), the simple depletion mechanism which assumes a total exclusion of polymer chains is unrealistic. Indeed, the polymer is small enough to swell the adsorbed surfactant brush and, possibly, be only partially excluded when two droplets approach. As an example, at the precipitation threshold corresponding to $n \approx 40$ ($\phi^* \approx 3\%$), the ideal-gas osmotic pressure is $22 \times 10^3\,\text{Pa}$. For this system, the radius of gyration is about 15 Å, leading to a depletion contact potential of about $10kT$. As seen in Fig. 3.8 (inset), for $n \approx 40$ the data do not agree with the scaling described above and, accordingly, the deduced contact potential at the threshold is much larger than kT. This suggests that the hard-core depletion mechanism is not realistic anymore. Indeed, such a mechanism overestimates the pair interaction at the precipitation threshold, and this overestimation becomes more dramatic as n decreases. For the same reasons, the slope of $\phi^*(n)$ for $n < 100$ deviates from the prediction based on that mechanism.

3.1.2 Models for Phase Transitions

An analogy may be drawn between the phase behavior of weakly attractive monodisperse dispersions and that of conventional molecular systems, pro-

vided coalescence and Ostwald ripening do not occur. The similarity arises from the common form of the pair potential, whose dominant feature in both cases is the presence of a shallow minimum. The equilibrium statistical mechanics of such systems has been extensively explored in recent years. The primary difficulty in predicting equilibrium phase behavior lies in the many-body interactions intrinsic to any condensed phase. Fortunately, a synthesis of several methods (integral-equation approaches, perturbation theories, virial expansions, and computer simulations) now provides accurate predictions of the thermodynamic properties and phase behavior of dense molecular fluids or colloidal fluids.

Freezing and crystallization are generally driven by potential minima that overcome the entropic tendency towards disorder. In some cases, however, entropy can actually induce order and cause a simple liquid to freeze. While this seems to go against intuition, such an entropy-driven freezing transition has been observed in computer simulations of spheres interacting through a purely repulsive hard-sphere potential [14]. Recently, this freezing transition has been observed experimentally in monodisperse, hard-sphere colloidal suspensions [15]. For liquids and suspensions made of single-size spheres, freezing is observed when the volume fraction ϕ of spheres exceeds approximately 0.494, and melting is observed at volume fractions lower than 0.545. In addition, it is now well established from theory and numerical simulations that the topology of the phase diagram depends on the ratio ξ of the interparticle attraction range Δ) to the interparticle hard-core repulsion range R, i.e. $\xi = (\Delta/R)$ [16, 17, 18, 19]. In the case of sufficiently small ξ, theory predicts that the only effect of the interparticle attraction is to expand the above-mentioned fluid–crystal coexistence region ($0.494 < \phi < 0.545$) (Fig. 3.9a). For ξ values larger than approximately 0.3, in addition to the fluid–solid coexistence region, a fluid–fluid coexistence (gas–liquid) is also predicted (Fig. 3.9b). Experimental evidence for the effect of the range of the interparticle attraction on equilibrium phase behavior has been provided by recent work on colloid–polymer and colloid–colloid mixtures [20, 21, 22, 23, 24], confirming the predicted topologies as a function of ξ. So far, in the field of emulsions, the only type of equilibrium that has been recognized is fluid–solid-like, which suggests that only small ξ values have been explored. This is most probably due to the fact that emulsion droplets have a characteristic diameter that generally lies in the range between 0.1 and 1 micron, a size which is much larger than the range of classical interactions.

3.2 Gelation and Kinetically Induced Ordering

Adhesive emulsion droplets stick to one another as they collide owing to their diffusive motion. As shown in Fig. 3.10, the resultant bonds can be sufficiently strong to prevent further rearrangements, leading to highly disordered, tenuous clusters, whose structure can be well described as fractal [25]. If there

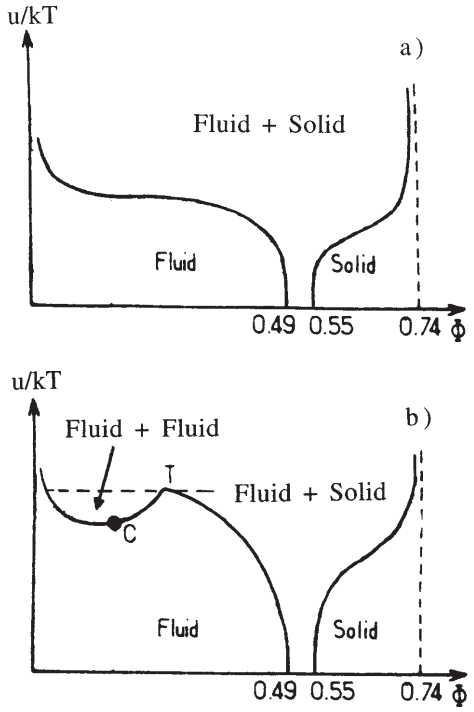

Fig. 3.9. Phase diagrams of attractive monodisperse dispersions: u is the contact pair potential and ϕ is the particle volume fraction. For $u/kT = 0$, the only phase transition accessible is the hard-sphere transition. If $u/kT \neq 0$, two distinct scenarios are possible according to the value of the ratio ξ (the range of the pair potential devided by the particle diameter). For $\xi < 0.3$ (**a**), only a fluid–solid equilibrium is predicted. For $\xi > 0.3$ (**b**), in addition to the fluid–solid equilibrium, a fluid–fluid (liquid–gas) coexistence is predicted with a critical point (C) and a triple point (T)

is no repulsive barrier preventing clusters from sticking upon collision, the coarsening of the emulsion is driven solely by the diffusion-induced collisions between the growing clusters. This regime, called diffusion-limited cluster aggregation (DLCA), is amenable to detailed theoretical analysis, and has become an important base case on which we can build our understanding of other kinetic growth processes. DLCA is completely random; nevertheless, recent experiments, with slightly more concentrated suspensions than previously studied, have shown that a surprising order can develop, manifested by a pronounced peak in the small-angle scattering intensity as a function of wave vector, $I(q)$, which reflects the development of a characteristic length scale in the suspension [26, 27, 28]. At long times, DLCA must produce a gel which spans the system, preventing further coarsening.

The structure of adhesive emulsions stabilized with an ionic surfactant in the presence of salt has been studied using light scattering [27, 28]. These emulsions are ideal systems for reaching the limit of DLCA as the droplets can be made unstable towards aggregation by temperature quenches. Before the quench, at high temperature, the droplets are homogeneously dispersed,

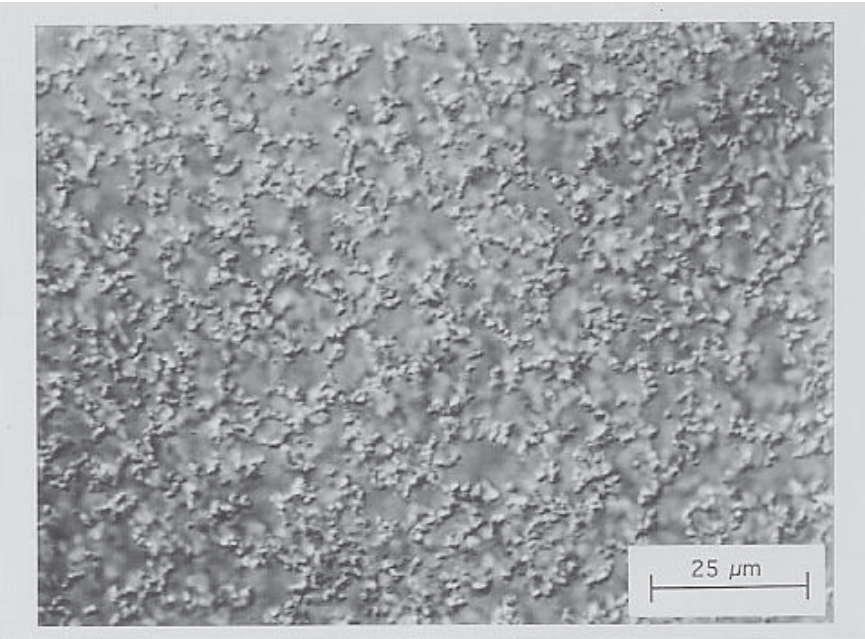

Fig. 3.10. Emulsion gel. The droplets are about 0.5 microns in diameter. They form large and ramified aggregates. Scale bar 25 μm

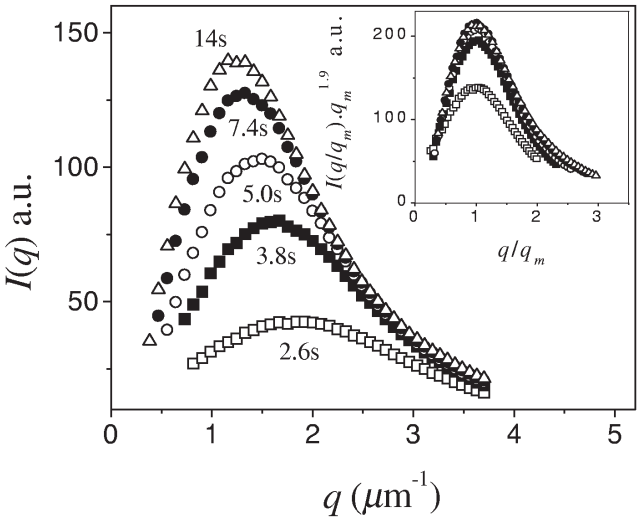

Fig. 3.11. Light-scattering intensity as a function of the wave vector for an emulsion with $\phi_0 = 0.04$ at a series of times. The *inset* shows that, except at the earliest times, the data can be scaled onto a single curve

whereas they stick to one another just after the quench. We plot in Fig. 3.11 a series of $I(q)$ curves taken at different times after the aggregation began using a sample with an initial droplet volume fraction of $\phi_0 = 0.04$; $t = 0$ has been chosen as the time when the first perceptible change in the scattering intensity is observed. There is a pronounced peak in $I(q)$ which grows in intensity and moves to lower q with time; ultimately the system gels, and

there are no further changes in $I(q)$. The scattering wave vector corresponding to the maximum intensity defines a characteristic length scale of the system, q_{m}^{-1}; at gelation, this length scales as q_{g}^{-1}. As has been observed previously [26], after a brief initial stage, all the scattering curves can be scaled onto a master curve by plotting $q_{\mathrm{m}}^{d_{\mathrm{f}}} I(q/q_{\mathrm{m}})$ as a function of q/q_{m}, where d_{f} is the fractal dimension of the clusters. This scaling is illustrated in the inset of Fig. 3.11, where we have used $d_{\mathrm{f}} = 1.9$. This value is close to 1.8, the expected value for DLCA [25]. Such scaling behavior has also been observed in other three-dimensional [26] and two-dimensional [29] colloidal systems. Several authors have pointed out the intriguing similarity between DLCA and spinodal decomposition, where scaling behavior is also observed [26, 29, 30, 31, 32]. Numerical simulations [30, 31, 32] and theoretical analysis [33] agree with the experimental results obtained with different systems. The peak is mainly due to a depletion shell around the larger clusters that is formed as aggregation proceeds [26]. However, at higher volume fractions and later times, the peak originates mainly from correlations between the growing clusters.

Moreover, for diffusion controlled gelation, we expect $q_{\mathrm{g}} \sim \phi_0^{1/(3-d_{\mathrm{f}})}$ [27, 28]; this is observed, as shown by the dashed line in Fig. 3.12, which is a fit to a power-law dependence of q_{g} on ϕ_0 for the data with $\phi_0 < 0.1$. The exponent is 0.75, close to the expected value, 0.83, for $d_{\mathrm{f}} = 1.8$. However, for $\phi_0 > 0.1$, there is a sharp change, and very little variation of q_{g} with ϕ_0 is observed. The origin of this behavior, like the mechanisms of colloidal aggregation at very high volume fractions, is still the subject of current research. Recent results show that the similarity to spinodal decomposition tends to be more pronounced in these regimes of highly concentrated systems [34]. There is still a pronounced peak in $I(q)$; however, q_{m} is independent of t, as shown

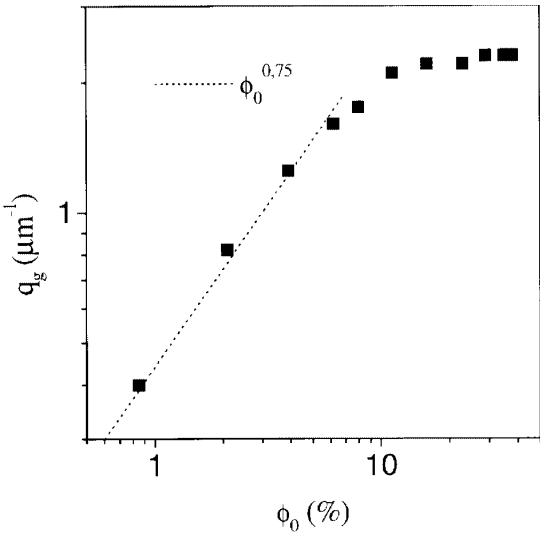

Fig. 3.12. The dependence of q_{g} on ϕ_0. For $\phi_0 < 0.1$, the data have a $\phi_0^{0.75}$ dependence, consistent with DLCA clusters with a fractal dimension of $d_{\mathrm{f}} = 1.9$

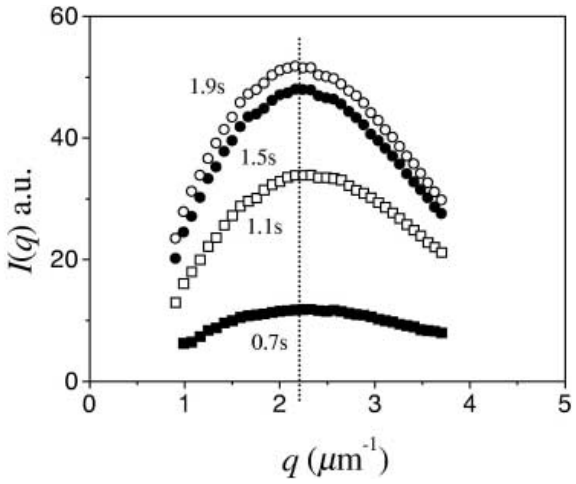

Fig. 3.13. Time evolution of $I(q)$ for $\phi_0 = 0.23$. The peak position does not change

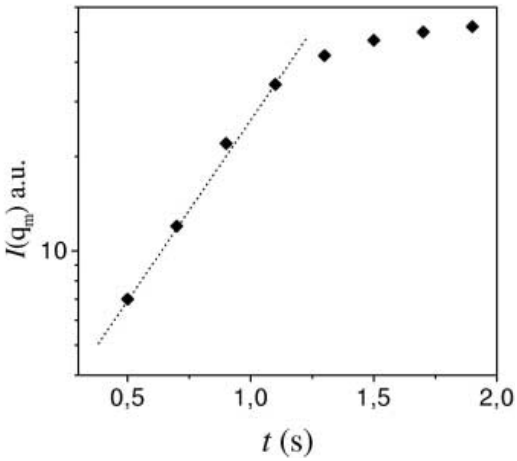

Fig. 3.14. Time evolution of the peak of $I(q)$ for $\phi_0 = 0.23$. The intensity increases exponentially with time till gelation is reached, in typically less than 2 s

in Fig. 3.13 for $\phi_0 = 0.23$. Moreover, the intensity at q_m grows exponentially with time until gelation occurs, typically in less than 2 s; this is shown in Fig. 3.14. Similar behavior is observed for all $\phi_0 > 0.1$, although the peak in $I(q)$ becomes broader as ϕ_0 is increased. This broadening is noticeably more pronounced when $\phi_0 > 0.3$. For $\phi_0 > 0.4$, a peak is no longer observed. The behavior in this second scenario is similar to that expected for the early stages of a spinodal decomposition within the framework of the Cahn–Hilliard linear theory [35, 36].

Finally, an important feature of gels made from adhesive emulsions arises from the deformation of the droplets. As the temperature is lowered, the contact angles between the droplets increase [27, 28]. Consequently, the structures of the final flocs depends on the time evolution of the strength of the adhesion. Initially, the adhesion results in the formation of a random, solid

gel network in the emulsion. Further, increase of adhesion causes massive fracturing of the gel, disrupting the rigidity of the structure and leading to well-separated, more compact flocs [27, 28].

References

1. S. Asakura, J. Oosawa: Interaction between particles suspended in solutions of macromolecules, J. Polym. Sci. **32**, 183 (1958) 47
2. M. P. Aronson: The role of free surfactont in destabilizing oil-in-water emulsions, Langmuir **5**, 494 (1989) 48
3. J. Bibette, D. Roux, F. Nallet: Depletion interactions and fluid-solid equilibrium in emulsions, Phys. Rev. Lett. **65**, 2470 (1990). 48
4. J. Bibette: Depletion interactions and fractionated crystallization for polydisperse emulsion purification, J. Colloid Interface Sci. **147**, 474 (1991) 48
5. J. Bibette, D. Roux, B. Pouligny: Creaming of emulsions: the rote of depletion forces induced by surfactant, J. Phys. II (France) **2**, 401 (1992) 50, 51
6. A. Meller, J. Stavans: Stability of emulsions with nonadsorbing polymers, Langmuir **12**, 301 (1996) 52
7. U. Steiner, A. Meller, J. Stavans: Entropy driven phase Separation in binary emulsions, Phys. Rev. Lett. **74**, 4750 (1995) 52
8. V. Digiorgio, R. Piazza, M. Corti, C. Minero: Critical properties of nonionic micellar solutions, J. Chem. Phys. **82**, 1025 (1984) 52
9. J. N. Israelachvili: *Intermolecular and Surface Forces* (Academic Press, New York 1992) 52, 56
10. F. Leal-Calderon, B. Gerhardi, A. Espert, F. Brossard, V. Alard, J. F. Tranchant, T. Stora, J. Bibette: Aggregation phenomena in Water-in-Oil emulsions, Langmuir **12**, 872 (1996) 53
11. B. P. Binks, P. D. I. Fletcher, D. I. Horsup: Effect of microemulsified surfactant in destabilizing water-in-oil emulsions containing C12E4, Colloids Surf. **61**, 291 (1991) 53
12. F. Leal-Calderon, O. Mondain-Monval, K. Pays, N. Royer, J. Bibette: Water-in-Oil emulsions: Role of the solvent molecular size an droplet interactions, Langmuir **13**, 7008 (1997) 55
13. P. G. De Gennes: *Scaling Concepts in Polymer Physics* (Cornell University Press, London 1979) 58
14. J. P. Hansen, I. R. McDonald: *Theory of Simple Liquids* (Academic Press, London 1991) 59
15. P. N. Pusey, W. van Megen: Phase behaviour of concentrated suspensions of nearly hard colloidal spheres, Nature **320**, 340 (1986) 59
16. A. P. Gast, C. K. Hall, W. B. Russel: Polymer-induced phase separations in non-aqueous colloidal suspensions, J. Colloid Interface Sci. **96**, 251 (1983) 59
17. B. Vincent, J. Edwards, S. Emmett, R. Croot: Phase Separation in dispersions of weakly interacting particles in solutions of non adsorbing polymer, Colloids Surf. **31**, 267 (1988) 59
18. H. N. W. Lekkerkerker, W. C. K. Poon, P. N. Pusey, A. Stroobants, P. B. Warren: Phase behaviour of colloid and polymer mixtures, Europhys. Lett. **20**, 59 (1992) 59

19. M. H. J. Hagen, D. Frenkel: Determination of phase diagrams for the hord-core attractive Yukawa System, J. Chem. Phys. **101**, 4093 (1994) 59
20. P. R. Sperry: Morphology and mechanism in latex flocculated by volume restriction, J. Colloid Interface Sci. **99**, 97 (1984) 59
21. B. Vincent: The Stability of non-aqueous dispersions of weakly interacting particles, Colloids Surf. **24**, 269 (1987) 59
22. F. Leal-Calderon, J. Bibette, J. Biais: Experimental phase diagrams of polymer and colloid mixtures, Europhys. Lett. **23**, 653 (1993) 59
23. W. C. K. Poon, S. M. Ilet, P. N. Pusey: Phase bahaviour of colloid-polymer mixture, Il nuovo cimento D **116**, 1127 (1994) 59
24. S. Sanyal, N. Easwear, S. Ramaswamy, et al. : Phase separation in binary nearly-hard-sphere colloids: evidence for the depietion force, Europhys. Lett. **18**, 107 (1993) 59
25. R. Jullien, R. Botet, *Aggregation and Fractal Aggregates* (World Scientific, Singapore 1987) 59, 62
26. M. Carpineti, M. Giglio: Spinodal-type dynamics in fractal aggregation of colloidal clusters, Phys. Rev. Lett. **68**, 3327 (1992) 60, 62
27. J. Bibette, T. G. Mason, H. Gang, D. A. Weitz: Kinetically induced ordering in gelation of emulsions, Phys. Rev. Lett. **69**, 981 (1992) 60, 62, 63, 64
28. J. Bibette, T. G. Mason, H. Gang, D. A. Weitz, P. Poulin: Structure of adhesive emulsions, Langmuir **9**, 3352 (1993) 60, 62, 63, 64
29. D. J. Robinson, J. C. Earnshaw: Long range order in two dimensional fractal aggregation, Phys. Rev. Lett. **71**, 715 (1993) 62
30. A. Hasmy, E. Anglaret, M. Foret, J. Pellows, R. Jullien: Small-angle neutron-scattering investigation of long-range correlations in silica aerogels: Simulations and experiments, Phys. Rev. B **50**, 6006 (1994) 62
31. A. Hasmy, R. Jullien: Sol-gel process simulation by cluster-cluster aggregation, J. Non-Cryst. Solids **186**, 342 (1995) 62
32. A. E. Gonzalez, G. Ramirez-Santiago: Spatial Ordering and Structure Factor Scaling in the Simulations of Colloid Aggregation, Phys. Rev. Lett. **74**, 1238 (1995) 62
33. F. Sciortino, P. Tartaglia: Structure Factor Scaling during Irreversible Cluster-Cluster Aggregation, Phys. Rev. Lett. **74**, 282 (1995) 62
34. P. Poulin, J. Bibette, D. A. Weitz: From colloidal aggregation to spinodal decomposition in sticky emulsions, Eur. J. Phys. B **9**, 3352 (1999) 62
35. J. M. Gunton, M. San Miguel, P. S. Sahni, In: C. Domb, J. L. Lebowitz (Eds.): *Phase Transition and Critical Phenomena* (Academic Press, London 1983), Vol. 8, p. 267 63
36. J. W. Cahn, J. E. Hilliard: Free Energy of a Nonuniform system. I. Interfacial Free Energy, J. Chem. Phys. **28**, 258 (1958) 63

Springer Tracts in Modern Physics

141 **Disordered Alloys**
Diffusive Scattering and Monte Carlo Simulations
By W. Schweika 1998. 48 figs. X, 126 pages

142 **Phonon Raman Scattering in Semiconductors, Quantum Wells and Superlattices**
Basic Results and Applications
By T. Ruf 1998. 143 figs. VIII, 252 pages

143 **Femtosecond Real-Time Spectroscopy of Small Molecules and Clusters**
By E. Schreiber 1998. 131 figs. XII, 212 pages

144 **New Aspects of Electromagnetic and Acoustic Wave Diffusion**
By POAN Research Group 1998. 31 figs. IX, 117 pages

145 **Handbook of Feynman Path Integrals**
By C. Grosche and F. Steiner 1998. X, 449 pages

146 **Low-Energy Ion Irradiation of Solid Surfaces**
By H. Gnaser 1999. 93 figs. VIII, 293 pages

147 **Dispersion, Complex Analysis and Optical Spectroscopy**
By K.-E. Peiponen, E.M. Vartiainen, and T. Asakura 1999. 46 figs. VIII, 130 pages

148 **X-Ray Scattering from Soft-Matter Thin Films**
Materials Science and Basic Research
By M. Tolan 1999. 98 figs. IX, 197 pages

149 **High-Resolution X-Ray Scattering from Thin Films and Multilayers**
By V. Holý, U. Pietsch, and T. Baumbach 1999. 148 figs. XI, 256 pages

150 **QCD at HERA**
The Hadronic Final State in Deep Inelastic Scattering
By M. Kuhlen 1999. 99 figs. X, 172 pages

151 **Atomic Simulation of Electrooptic and Magnetooptic Oxide Materials**
By H. Donnerberg 1999. 45 figs. VIII, 205 pages

152 **Thermocapillary Convection in Models of Crystal Growth**
By H. Kuhlmann 1999. 101 figs. XVIII, 224 pages

153 **Neutral Kaons**
By R. Belušević 1999. 67 figs. XII, 183 pages

154 **Applied RHEED**
Reflection High-Energy Electron Diffraction During Crystal Growth
By W. Braun 1999. 150 figs. IX, 222 pages

155 **High-Temperature-Superconductor Thin Films at Microwave Frequencies**
By M. Hein 1999. 134 figs. XIV, 395 pages

156 **Growth Processes and Surface Phase Equilibria in Molecular Beam Epitaxy**
By N.N. Ledentsov 1999. 17 figs. VIII, 84 pages

157 **Deposition of Diamond-Like Superhard Materials**
By W. Kulisch 1999. 60 figs. X, 191 pages

158 **Nonlinear Optics of Random Media**
Fractal Composites and Metal-Dielectric Films
By V.M. Shalaev 2000. 51 figs. XII, 158 pages

159 **Magnetic Dichroism in Core-Level Photoemission**
By K. Starke 2000. 64 figs. X, 136 pages

160 **Physics with Tau Leptons**
By A. Stahl 2000. 236 figs. VIII, 315 pages

161 **Semiclassical Theory of Mesoscopic Quantum Systems**
By K. Richter 2000. 50 figs. IX, 221 pages

Springer Tracts in Modern Physics

162 **Electroweak Precision Tests at LEP**
By W. Hollik and G. Duckeck 2000. 60 figs. VIII, 161 pages

163 **Symmetries in Intermediate and High Energy Physics**
Ed. by A. Faessler, T.S. Kosmas, and G.K. Leontaris 2000. 96 figs. XVI, 316 pages

164 **Pattern Formation in Granular Materials**
By G.H. Ristow 2000. 83 figs. XIII, 161 pages

165 **Path Integral Quantization and Stochastic Quantization**
By M. Masujima 2000. 0 figs. XII, 282 pages

166 **Probing the Quantum Vacuum**
Pertubative Effective Action Approach in Quantum Electrodynamics and its Application
By W. Dittrich and H. Gies 2000. 16 figs. XI, 241 pages

167 **Photoelectric Properties and Applications of Low-Mobility Semiconductors**
By R. Könenkamp 2000. 57 figs. VIII, 100 pages

168 **Deep Inelastic Positron-Proton Scattering in the High-Momentum-Transfer Regime of HERA**
By U.F. Katz 2000. 96 figs. VIII, 237 pages

169 **Semiconductor Cavity Quantum Electrodynamics**
By Y. Yamamoto, T. Tassone, H. Cao 2000. 67 figs. VIII, 154 pages

170 **d–d Excitations in Transition-Metal Oxides**
A Spin-Polarized Electron Energy-Loss Spectroscopy (SPEELS) Study
By B. Fromme 2001. 53 figs. XII, 143 pages

171 **High-T_c Superconductors for Magnet and Energy Technology**
By B. R. Lehndorff 2001. 139 figs. XII, 209 pages

172 **Dissipative Quantum Chaos and Decoherence**
By D. Braun 2001. 22 figs. XI, 132 pages

173 **Quantum Information**
An Introduction to Basic Theoretical Concepts and Experiments
By G. Alber, T. Beth, M. Horodecki, P. Horodecki, R. Horodecki, M. Rötteler, H. Weinfurter, R. Werner, and A. Zeilinger 2001. 60 figs. XI, 216 pages

174 **Superconductor/Semiconductor Junctions**
By Thomas Schäpers 2001. 91 figs. IX, 145 pages

175 **Ion-Induced Electron Emission from Crystalline Solids**
By Hiroshi Kudo 2002. 85 figs. IX, 161 pages

176 **Infrared Spectroscopy of Molecular Clusters**
An Introduction to Intermolecular Forces
By Martina Havenith 2002. 33 figs. VIII, 120 pages

177 **Applied Asymptotic Expansions in Momenta and Masses**
By Vladimir A. Smirnov 2002. 52 figs. IX, 263 pages

178 **Capillary Surfaces**
Shape – Stability – Dynamics, in Particular Under Weightlessnes
By Dieter Langbein 2002. 182 figs. XVIII, 364 pages

179 **Anomalous X-ray Scattering for Materials Characterization**
Atomic-Scale Structure Determination
By Yoshio Waseda 2002. 55 figs. XIV, 214 pages

180 **Coverings of Discrete Quasiperiodic Sets**
Theory and Applications to Quasicrystals
Edited by P. Kramer and Z. Papadopolos 2002. 128 figs., XIV, 274 pages

181 **Emulsion Science**
Basic Principles. An Overview
By J. Bibette, F. Leal-Calderon, V. Schmitt, and P. Poulin 2002. 50 figs., IX, 140 pages